Surface Science 259 (1991) 235–252
North-Holland

surface science

Formation of a well-ordered aluminium oxide overlayer by oxidation of NiAl(110)

R.M. Jaeger, H. Kuhlenbeck, H.-J. Freund
Ruhr-Universität Bochum, Physikalische Chemie I, Postfach 102148, D-4630 Bochum, Germany

M. Wuttig, W. Hoffmann, R. Franchy and H. Ibach
Institut für Grenzflächenforschung und Vakuumphysik, Forschungszentrum Jülich, Postfach 1913, D-5170 Jülich, Germany

Received 18 March 1991; accepted for publication 3 July 1991

We have investigated the electronic and geometric structure of a thin oxide film grown by oxidation on NiAl(110) using electron spectroscopic techniques, i.e., LEED, EELS, XPS and ARUPS. This film is inert to adsorption of, respectively reaction with many molecules up to temperatures of about 800 K. It is well ordered as deduced from the LEED pattern and covers the whole surface. We find that the oxide film is about 5 Å thick, consisting of aluminium oxide as shown by EELS, XPS and ARUPS. It is most likely formed of two aluminium layers and two quasihexagonal oxygen layers with oxygen surface termination. Since the oxide film is rather thin it only shows a two-dimensional band structure which has been investigated using ARUPS. For the electronic levels of the oxide strong periodic dispersions are observed with bandwidths compatible to dispersion bandwidths calculated for the ΓX direction of α-Al_2O_3.

1. Introduction

Aluminium oxide is one of the most important supports for dispersed metal catalysts. If one intends to carry out model studies on well ordered oxide surfaces an electron spectroscopic characterization is essential. However, α-Al_2O_3 for example, is an insulator and it is rather problematic to study insulators with electron spectroscopic methods, although progress has been made in this direction [1]. It is therefore desirable from this and from various other points of view, e.g., for the study of buried metal–oxide interfaces, to be able to create a thin oxide film on a metal support with a well defined geometric and eletronic structure that is identical or close to the properties of the bulk oxide.

Concerning aluminium oxide it is known that it is possible to prepare thin films on top of aluminium single-crystal surfaces [2–8], but unfortunately these films do not exhibit a well-ordered geometric structure, i.e., they are amorphous oxide layers. In light of this problem the observation that the oxidation of the (110) surface of the body centered alloy NiAl leads to the formation of a well-ordered adsorbate film with high oxygen content is interesting [9–11]. It has been speculated that this film consists of aluminium oxide, but a more detailed characterization with respect to the geometric and electronic structure is still missing.

In the present paper we report the results of a combined LEED, ARUPS, XPS and EELS study and propose a structure which is basically that of a distorted hexagonal Al_2O_3 surface with a thickness of two oxygen/aluminium layers and oxygen surface termination.

The paper is organized by first presenting all the accumulated experimental evidences for the stoichiometry and the geometric and electronic

structure of the system. The results are then used to derive the structural model presented in the last section.

2. Experimental

The experiments were performed in two different ultrahigh vacuum (UHV) systems. Both systems were equipped with LEED, AES and a quadrupole gas spectrometer for residual gas analysis.

The UHV system used for the photoemission experiments (VG ADES 400) additionally contained a hemisperical electron energy analyser rotatable in two orthogonal planes for angular resolved photoelectron detection. Photoelectrons were excited with light from the TGM2 beamline at the BESSY synchrotron radiation center in Berlin.

The UHV system used for vibrational spectroscopy contained a high-resolution electron energy loss spectrometer which has been described elsewhere [12]. It is capable of a resolution below 16 cm^{-1} (2 meV) at high count rates. The EELS spectra presented in this study have typically been taken with a resolution of 25 cm^{-1}.

The NiAl(110) samples were oriented by stan-

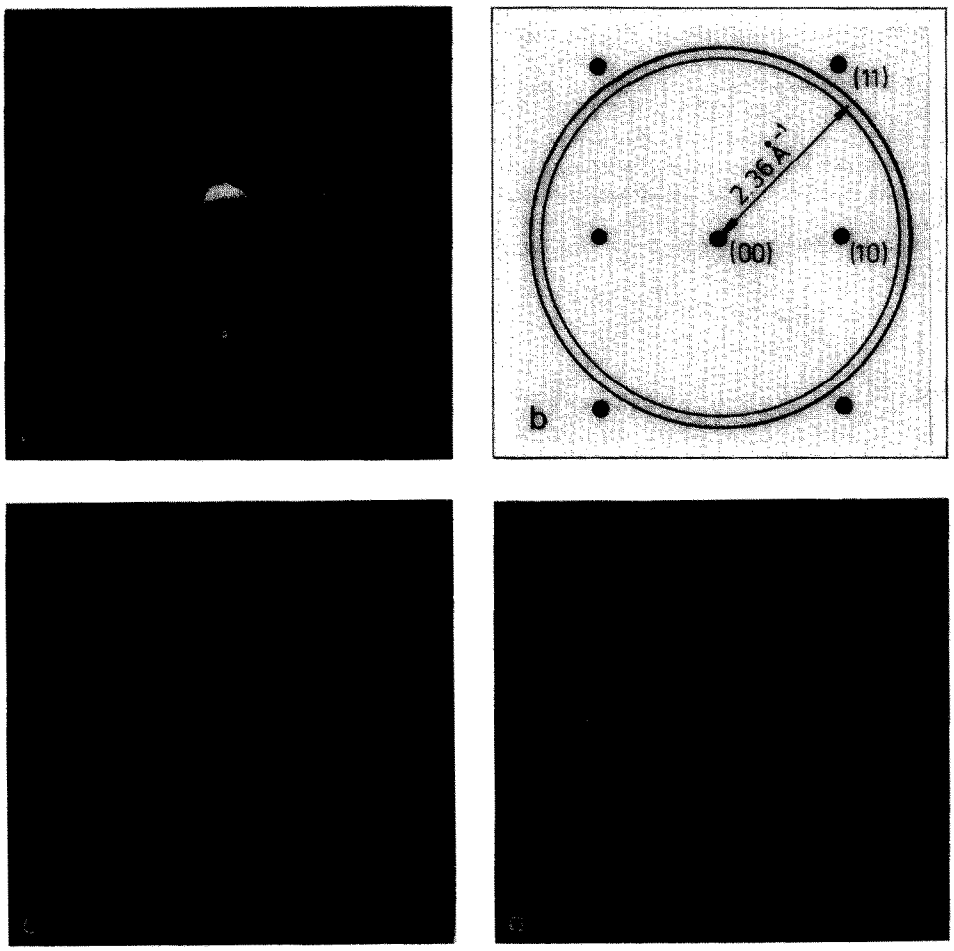

Fig. 1. LEED patterns for oxygen on NiAl(110). (a) NiAl(110) clean, $E_p = 61$ eV. (b) Dosed with 1200 L O_2 at room temperature and annealed to $T = 600$ K. (c) Annealed to $T = 1000$ K, $E_p = 46$ eV. (d) Annealed to $T = 1300$ K, $E_p = 46$ eV.

dard Laue technique with an accuracy of about 1°. After mechanical polishing the samples were cleaned in UHV by repeated cycles of sputtering with Ne ions and annealing to 1300 K. Residual carbon was then removed by cycles of heating to 1100 K in an oxygen atmosphere of 10^{-7} mbar with subsequent annealing to 1300 K. These cleaning cycles were repeated until LEED, AES, and EELS indicated a clean and well-ordered surface.

3. Results and discussion

3.1. LEED

NiAl forms an ordered alloy which crystallizes in the body-centered CsCl structure [13]. A LEED pattern of the (110) surface is shown in fig. 1a. It is known from the literature that the surface is buckled with the Al surface atoms displaced by 0.2 Å towards vacuum [14–16].

When the surface is exposed to increasing amounts of oxygen up to saturation (1200 L) at room temperature the substrate LEED spots become more and more diffuse until at saturation the substrate LEED spots are no longer visible on the screen. This means that the surface has lost long-range order within at least 5–7 Å perpendicular to the surface. Upon subsequent annealing to 600 K the substrate spots reappear and in addition a diffuse ring structure with an average radius of 2.36 $Å^{-1}$ is observed (see fig. 1b; the original photograph is not shown here because the ring structure is so weak that it might not be visible in the reproduction). Further annealing to 1000 K then leads to the following scenario: The substrate spots become more intense and the diffuse ring starts to break up into six ring fragments as shown in fig. 1c. Within the ring fragments a distinct spot structure is visible. The sharpening of this spot structure for the six ring fragments is complete at 1300 K and leads to the pattern shown in fig. 1d. There is, however, still a lot of diffuse intensity between the spots.

The diffuse ring structure observed at 600 K is indicative of an adsorbate layer with distinct domains of long-range order but random orientation with respect to the NiAl-substrate. It is most likely due to an overlayer with quasihexagonal symmetry as indicated by the six ring fragments in the LEED pattern shown in fig. 1c. The lattice constant of this overlayer as deduced from the ring diameter is 3.07 Å. In the following sections we shall see that the overlayer very likely consists of aluminium oxide terminated with a quasihexagonal oxygen layer.

With the appearance of the LEED pattern shown in fig. 1d the final state of surface oxidation has not yet been reached. Upon dosing 1200 L O_2 at $T = 550$ K and subsequent annealing to $T = 1200$ K the final LEED pattern is observed. It is shown in fig. 2a. As is obvious from the photograph the spots are very sharp which implies that we are dealing with a well-defined, long-range ordered structure. This pattern has been observed before [10,11], but so far it has not been possible to extract a sensible structure model in real space. Fig. 2b contains a schematic representation of the pattern. It reveals that the substrate spots are still present. The real-space unit mesh of the oxide film ($a = 10.55$ Å, $b = 17.88$ Å, $\alpha = 88.7°$) as determined by Müller and coworkers [10] is much larger than the one of the substrate ($a = 2.887$ Å, $b = 4.083$ Å, $\alpha = 90°$) [14,15]. These unit cells are also shown in fig. 2b. The angle between the unit vectors of the oxide is 88.7° and the mesh is rotated by about 24° with respect to the substrate mesh. As shown in ref. [10] the oxide film is commensurate with the substrate along the substrate [$1\bar{1}0$] direction and incommensurate along [001]. Due to the C_{2v} symmetry of the substrate we expect two domains of the overlayer to exist on the surface. They are marked in fig. 2b. With these domains all observed LEED spots may be explained. However, we note that we could not identify double-diffraction spots in the LEED pattern. Such spots should in principle exist since the oxide film is incommensurate with the substrate in one direction. A possible reason that we could not observe such spots is that they are too weak. The thickness of the film is about 5 Å which means that doubly diffracted electrons have to travel at least 10 Å through the oxide. This will decrease the intensity appreciably. As can be seen from the photograph

in fig. 2a the oxide film exhibits many spots. Thus the remaining intensity of the beam scattered by the substrate has to be distributed into many diffraction channels so that there will be not much intensity remaining for a single double-diffraction spot. This explains why the double-diffraction spots should be rather weak, but it remains a problem that we could not even identify weak indications of such spots in the photographs of the LEED patterns. One might suppose that there is some sort of interlayer between the NiAl substrate and the oxide film which is commensurate with the oxide film, possibly consisting of NiO or pure Ni. But, as will be shown in the following sections, we have spectroscopical evidence that such an interlayer does not exist. Another possible reason for the absence of double diffraction spots could be that the topmost

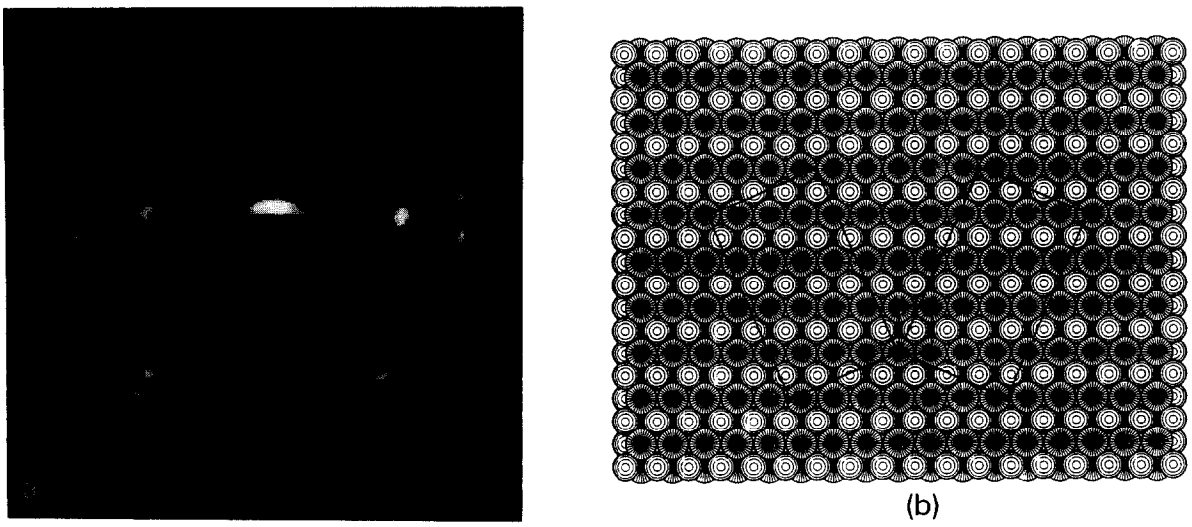

Fig. 2. (a) LEED pattern of Al_2O_3 on NiAl(110) obtained after dosing 1200 L O_2 at $T = 550$ K and subsequent annealing to $T = 1200$ K. (b) Real-space and reciprocal-space schematics of the oxide unit mesh as derived from the LEED pattern in the left panel [10].

layer(s) of the NiAl substrate below the oxide film are accommodated to the structure of the film such that the oxide film is commensurate with these layer(s). This might be in agreement with our data if these NiAl layer(s) are not too much distorted.

3.2. EELS

While LEED probes the long range order within the adsorbate film, EELS is more sensitive to the local arrangement on the surface. Fig. 3a shows a series of EELS spectra for increasing oxygen exposure at room temperature, and fig. 3b exhibits a set of spectra where the system giving rise to the upmost spectrum in fig. 3a has been annealed for one minute to different temperatures. There are several pieces of information contained in these spectra. First, with increasing oxygen coverage the elastic peak decreases in intensity by more than a factor of 5. Second, there are three features with loss energies above 300 cm^{-1} which change their frequencies with increasing coverage. The feature close to 215 cm^{-1} is due to a NiAl phonon discussed in detail elsewhere [17,18]. If we anneal the oxygen-

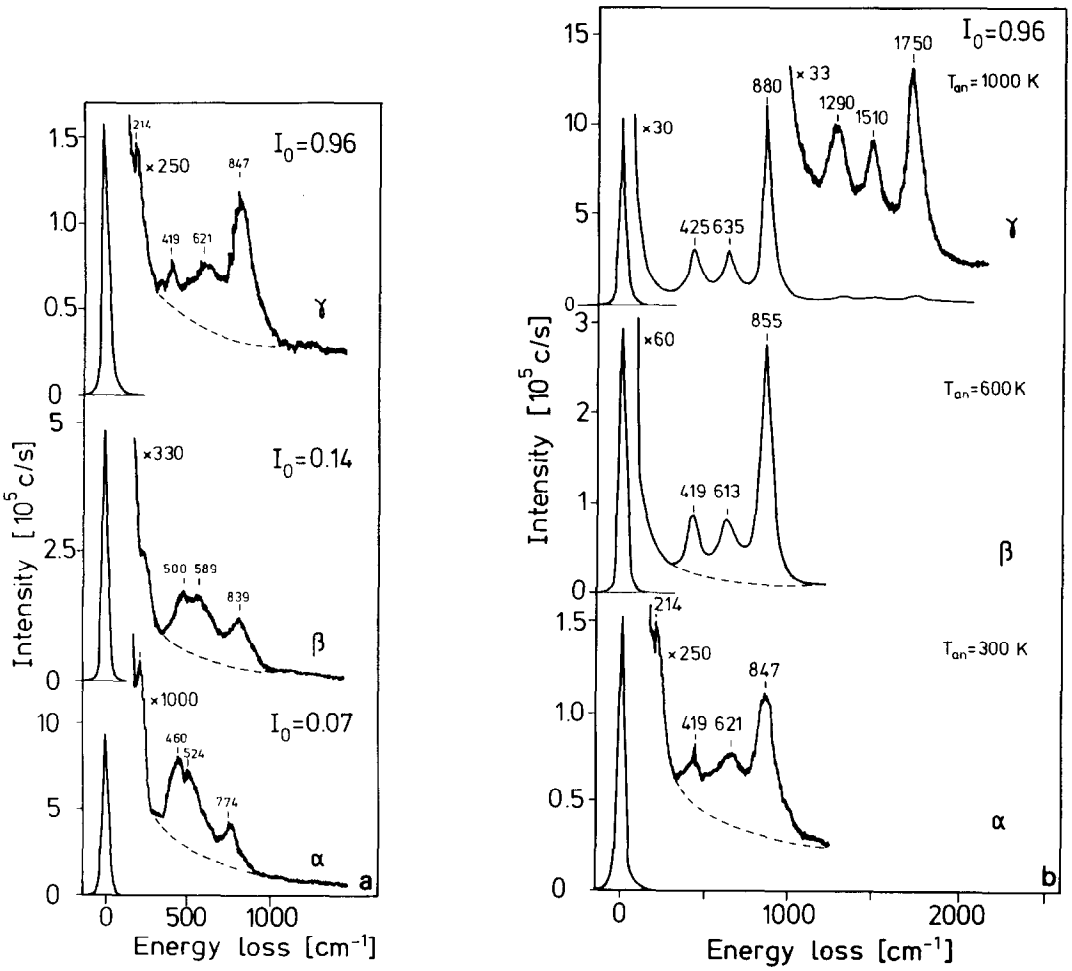

Fig. 3. EEL spectra for oxygen on NiAl(110) obtained for different conditions of prepations. (a) EEL spectra obtained for different exposures at room temperature. The I_0 values are the ratios of the oxygen Auger lines at 512 eV and the Ni Auger lines at 848 eV. (b) EEL spectra of NiAl(110) dosed with 1200 L O_2 at room temperature and subsequently annealed to different temperatures.

saturated surface, the intensity of the elastic beam is recovered and, simultaneously, the line widths of the loss features decrease while the frequencies remain about the same. In fact, we find that the integrated relative intensities of the bands remain constant for all annealing temperatures between 300 and 1300 K. Note, that in the final state, i.e., after annealing to 1000 K, the NiAl phonon is no longer observed. The upmost spectrum in fig. 3b corresponds to a surface with a LEED pattern shown in fig. 1d, i.e., the LEED pattern with the hexagon. The main conclusion from the results so far is that the local structure on the surface formed by saturation coverage of oxygen is the same for the disordered surface and for the well-ordered surface. Only at very low oxygen coverages (fig. 3a) do we seem to have a different local arrangement on the surface. However, upon annealing again a spectrum similar to spectrum γ in fig. 3a is observed, indicating the transformation into the particular local structure. This structure also characterizes the surface which has a LEED pattern as shown in fig. 2a. The corresponding EEL spectrum is shown in fig. 4. Even though this structure has been obtained after much higher oxygen exposures the same spectrum with peaks at 410, 620 and 850 cm^{-1} is observed. Even the intensity ratios of the EEL peaks closely resemble the EEL spectrum of the structure with the hexagonal LEED pattern [19].

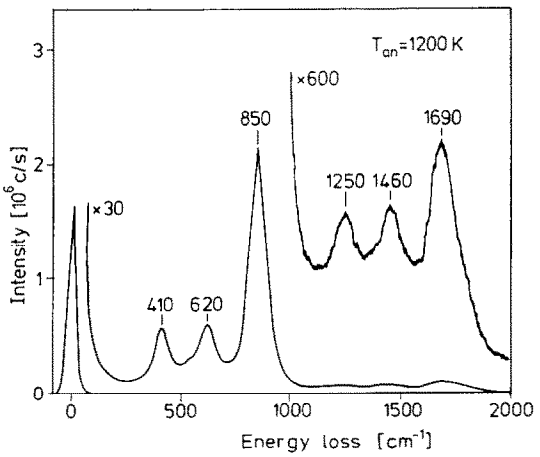

Fig. 4. EEL spectrum of the Al_2O_3 film on NiAl(110) with the LEED pattern shown in fig. 2a.

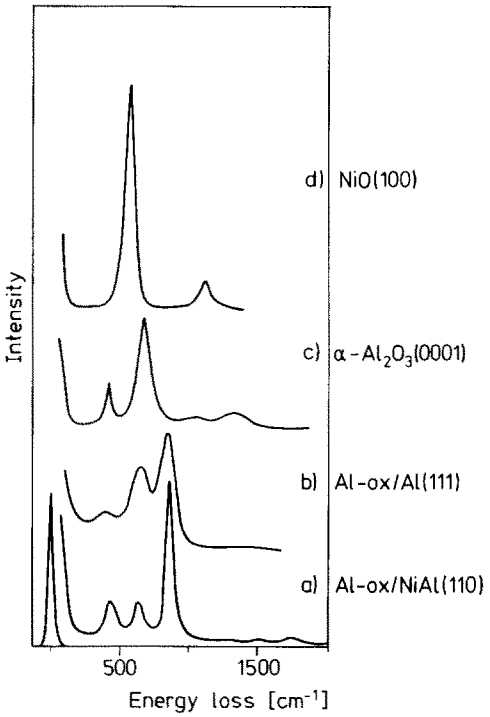

Fig. 5. EEL spectra of different oxides [2,23,24].

This indicates that the local structures on these differently prepared surfaces are very similar. Before we proceed with the assignment of the modes in the loss spectra we note, that very similar loss spectra are observed for oxygen adsorption on NiAl(111) after annealing to 1050 K [20].

The similarities between the oxygen-exposed NiAl(110) and NiAl(111) surfaces are already indicative of a particularly interesting aspect of the oxygen adsorption behaviour. It appears as if the oxygen only strongly interacts with one constituent of the alloy, similar to observations reported for the interaction of oxygen with Ni_3Al [21]. The rather large intensities of the loss features of the annealed, well ordered overlayer (see the multiple losses in fig. 3b, γ) are indicative of the formation of an oxide overlayer. Due to the strong metal–oxygen dipoles, oxide surfaces generally exhibit very intense loss features. In order to decide which oxide is formed on the surface spectrum γ of fig. 3b is compared with the EEL-spectra of NiO(100) [22,23], α-Al_2O_3(0001) [24] and a thin amorphous film of aluminium oxide on

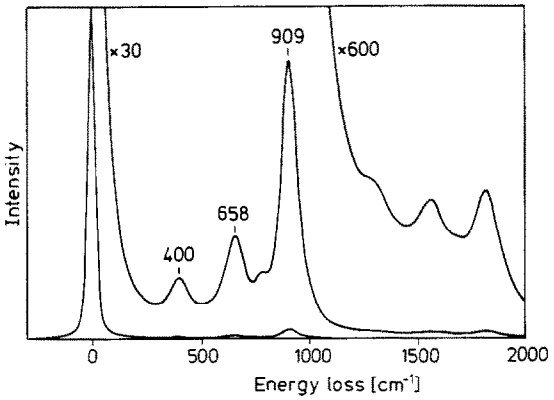

Fig. 6. Calculated EEL spectrum of a thin film of γ-Al_2O_3 on NiAl(110).

an Al(111) surface [2,3,6,8] in fig. 5. Clearly, by comparison the oxide overlayer on NiAl(110) is not a NiO overlayer. However, the α-Al_2O_3(0001) spectrum also does not appear to compare favourably. There are two loss features in the α-Al_2O_3 spectrum while there are three features observed for the oxide overlayer on NiAl(110). The α-Al_2O_3(0001) loss spectrum is well described in terms of dielectric theory as was shown by Liehr et al. [24]. For a thin film of α-Al_2O_3 on NiAl the loss spectra look slightly different, i.e., the loss peaks are shifted as compared to the loss features of bulk α-Al_2O_3, but no new mode appears [25]. On the other hand loss spectra calculated by dielectric theory for a thin film of γ-Al_2O_3 on Al [26] and on NiAl (fig. 6, parameters have been taken from ref. [27]) resemble the measured spectra closely. These calculations show peaks at 400, 660 and 910 cm^{-1}. Similar spectra have been observed for thin aluminium oxide films on an Al(111) substrate. The loss features of such a thin film favourably compare with the present system as is evident from fig. 5. Strong et al. [6] have interpreted the aluminium oxide/Al(111) loss features via lattice-dynamical model calculations and suggest that the three modes are derived from the correlated motion of two aluminium and two oxygen layers arranged as alternating layers. The model calculations indicate that the two high-energy modes between 500 and 1000 cm^{-1} are produced by oxygen atoms vibrating 180° out of phase with neighboring Al atom planes. This corresponds to relatively large dynamic dipole moments and therefore larger intensities. The mode below 500 cm^{-1} is produced by an in-phase oscillating Al/O sandwich vibrating 180° out of phase with the second Al/O sandwich. The relative amplitude for this mode can be expected to be smaller. This means that the appearance of three loss features is indicative of a peculiar vibrational coupling between two distinct Al/O-sandwiches. Therefore the observed loss spectrum is characteristic of a very thin aluminium oxide film consisting of two oxygen/aluminium bilayers.

Recently, this assignment has been questioned by Yates and coworkers [28]. They investigated thin films of Al_2O_3 on Mo(110) and found that the low-frequency mode at 400 cm^{-1} should be due to an incomplete oxidation of the aluminium. On the other hand Rhodin and coworkers [26] obtained the result that this mode should be an intrinsic mode of stoichiometric Al_2O_3. The latter is most probably also valid in the case of Al_2O_3 on NiAl(110) since if there were defects consisting of unoxidized Al atoms randomly distributed in the oxide lattice we should observe this in the LEED pattern. There should be a high background intensity and the spots would possibly be not as sharp as they are (see fig. 2a). Besides this we note that the mode at 400 cm^{-1} is always present for γ-Al_2O_3 (see fig. 6).

3.3. AES/XPS and thermodynamics

Isern and Castro performed an AES-study of the oxygen uptake on NiAl(110) [11]. From the analysis of their Auger data they concluded, that Ni remains chemically unaffected by the presence of oxygen, while the position of the Al-LMM transitions indicates the formation of Al^{3+} as in Al_2O_3. The authors were able to estimate the thickness of the Al_2O_3 layer at oxygen saturation to be 5 Å. The Auger spectra taken in the present study are rather similar to those taken by Isern and Castro for the oxygen-saturated surface and allow us to estimate a thickness of the oxide layer of 5 ± 1 Å, in good agreement with the previously reported value. While the Auger data only suggest the presence of oxide on the surface

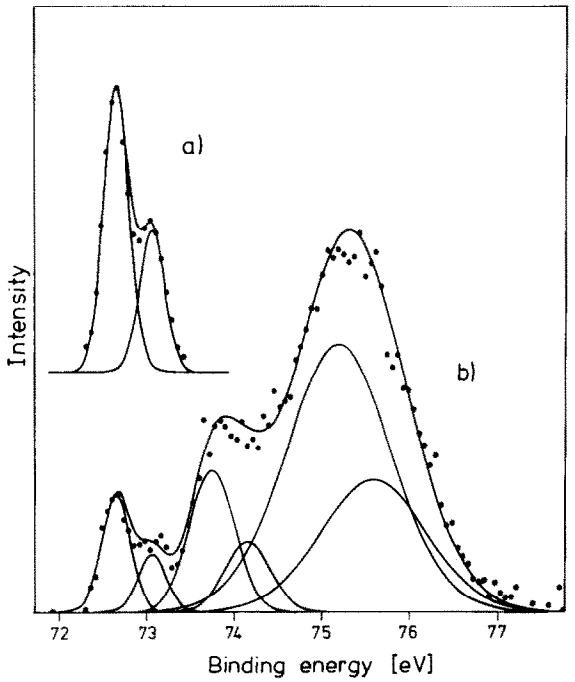

Fig. 7. Al2p XP spectra obtained at $\hbar\omega = 120$ eV. (a) NiAl(110) clean. (b) Aluminium oxide on NiAl(110). The LEED pattern of the oxide was that shown in fig. 2a.

without allowing any further analysis as to whether there are possibly different Al species within the oxide overlayer, photoelectron spectroscopy of the Al 2p levels recorded at a resolution of 0.3 eV employing synchrotron radiation leads to a more detailed picture. The spectrum of clean NiAl(110) is shown in fig. 7a. The spectrum was recorded at normal emission with a photon energy of 120 eV, i.e., close to the minimum of the electron escape depth versus E_{kin} curve. The Al 2p exhibits the doublet due to the final Al $2p_{1/2}$ and Al $2p_{3/2}$ states with the expected intensity ratio of 1:2 between the two spin–orbit components which are split by 0.4 eV [29–32]. Upon oxygen saturation and subsequent annealing the Al 2p spectrum becomes very complex. Table 1 lists the experimentally determined energy positions. At the lowest binding energy the doublet due to Al in NiAl is still visible. We assign the features at higher binding energies to aluminium species in the Al-oxide overlayer. As is obvious from the spectra there are at least two different aluminium species present in the oxide. Concerning for instance γ-Al_2O_3 this may be connected with the fact that in this oxide two differently coordinated sorts of Al atoms exist, i.e., tetrahedrally coordinated ions and octahedrally coordinated ions, and that not all of the Al positions are occupied [33]. Another possible reason is that part of the Al atoms are in direct contact with the NiAl substrate which also would influence the Al 2p binding energy. A more elaborate angle dependent XPS study on this problem should help us to adress this problem in more detail.

Table 1
Al2p peak positions for Al_2O_3 on NiAl(110) (the numbers have been obtained by a fit of the XP spectrum shown in fig. 7b)

	NiAl	Al_2O_3	
Al $2p_{3/2}$	72.68	73.75	75.17
Al $2p_{1/2}$	73.08	74.17	75.60

From a thermodynamic point of view the formation of an Al_2O_3 oxide overlayer is energetically strongly favoured over the formation of a NiO overlayer because the heat of formation for Al_2O_3 (−1690.7 kJ/mol) [34] is by a factor of seven larger than the corresponding value for NiO (−240.8 kJ/mol) [34]. On the other hand the energy necessary to form elemental Ni and Al from NiAl is only 58.8 kJ/mol [35,36]. Therefore a reaction of the form

$$2\,NiAl_{(s)} + \tfrac{3}{2}O_{2(g)} \rightarrow 2\,Ni_{(s)} + Al_2O_{3(s)},$$

where two NiAl layers react with oxygen to form Al_2O_3 and two equivalents of Ni is strongly exothermic. Even though the above arguments are exclusively based on enthalpy arguments we do not expect that the inclusion of entropic terms changes the overall picture significantly.

3.4. Angle-resolved photoemission

Fig. 8a shows a valence-band photoelectron spectrum of the clean NiAl(110) surface in normal emission. A similar spectrum and a complete band structure study of NiAl(110) have been published before by Plummer and coworkers [37,40]. Spectra 8b and 8c have been taken after oxygen

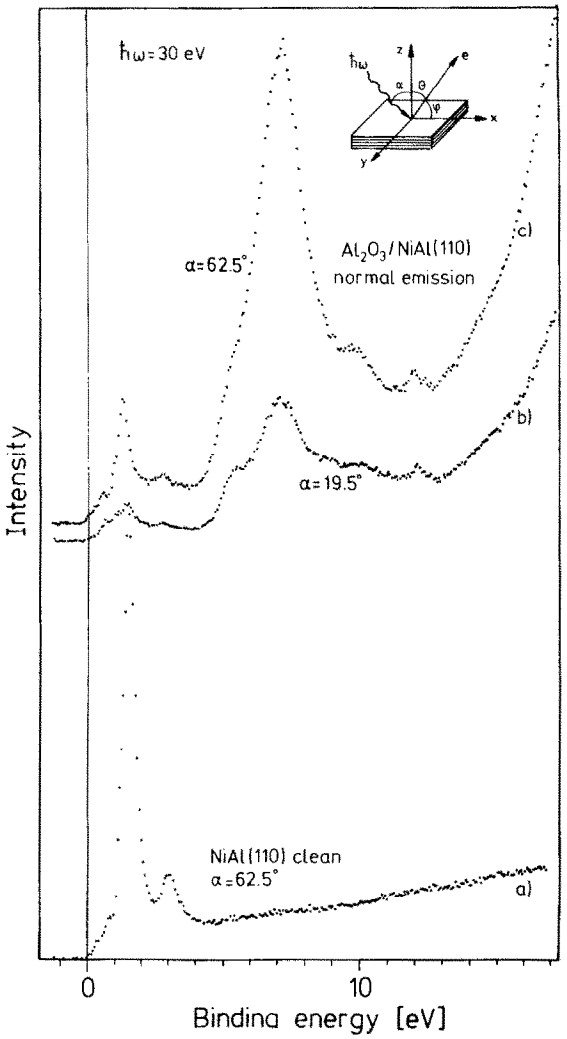

Fig. 8. Normal emission UP spectra of clean and oxygen-covered NiAl(110). The LEED pattern of the oxide was that shown in fig. 2a.

treatment which leads to our final LEED pattern. Strong emissions are observed between 4 and 13 eV binding energy due to the formation of oxygen induced states. Two spectra are shown, one excited with mainly z-polarized light, i.e., light polarized perpendicular to the surface (spectrum c), and another one excited with mainly s-polarized light, i.e., light polarized parallel to the surface. Considering both spectra we can identify five features due to emission of the oxide. These are found at 5, 7, 8.5, 10.0 and 12 eV varying slightly with polarization in relative intensity.

The spectra clearly reveal that there is no NiO formed within the detection limit of our spectrometer. The photoelectron spectra of ordered bulk NiO as well as those of thin NiO films have been investigated in detail in the past [23,41]. The presence of NiO would lead to intense emission in the region between the Fermi energy and 5 eV binding energy differing significantly from the NiAl emission. However, the present data do not indicate such NiO build up at all. Also the existence of elemental Ni can be excluded since this would lead to intense Ni d-band emission directly at the Fermi edge which is not observed in the spectra. The features between the Fermi edge and 5 eV binding energy in figs. 8b and 8c look just like the emissions of the clean NiAl(110) surface shown in fig. 8a, so that there is no evidence for the existence of a Ni or NiO interlayer between the aluminium oxide film and the NiAl(110) substrate.

Fig. 9 collects a set of spectra taken at normal emission with different photon energies and in fig. 10 a set of spectra taken at different electron exit angles in the [1$\bar{1}$0] azimuth is shown. Whereas the spectra taken at different photon energies probe the band structure of the oxide along a direction in k-space perpendicular to the surface in the spectra taken at different detection angles also the k-vector parallel to the surface is varied. In fig. 10 strong band dispersions are observed with bandwidths similar to calculated bandwidths for the ΓM direction of α-Al_2O_3 [42]. On the other hand the dispersion bandwidths in the spectra of fig. 9 are near to zero. This means that the oxide film has developed a well-defined band structure in directions parallel to the surface whereas perpendicular to the surface only very weak indications of dispersions exist. It is known from the literature [43] that for a thin epitaxial Ni film on W(110) a three-dimensional band structure begins to develop at film thicknesses of about 2 monolayers. In this context the observation that only weak dispersions are observed as a function of photon energy is a consequence of the limited thickness of the film which was determined to be about 5 Å which approximately corresponds to two aluminium/oxygen bilayers.

The attenuation of the oxygen induced fea-

tures with increasing photon energy (fig. 9) is quite typical and reflects the decrease of the cross-section of atomic oxygen relative to the Ni 3d cross section. The latter electrons are the dominant contributors to the valence band emission intensity of NiAl for all photon energies.

Concerning the overall variation of the intensities of the oxygen levels versus the NiAl states in fig. 10 it is clear from the data that the oxygen

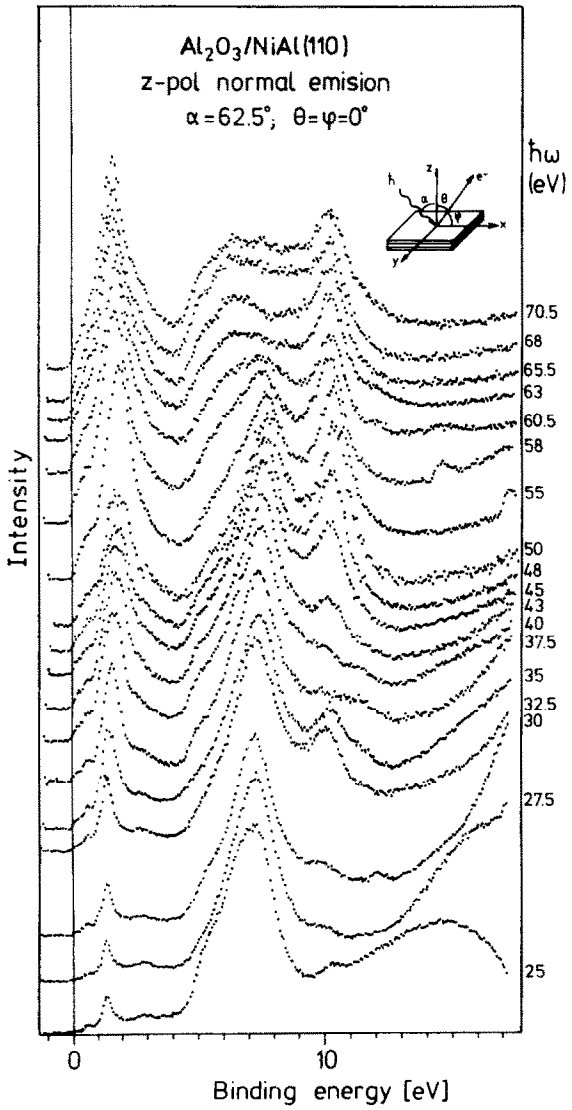

Fig. 9. Series of UP spectra of Al_2O_3/NiAl(110) (LEED pattern shown in fig. 2a) obtained for different photon energies.

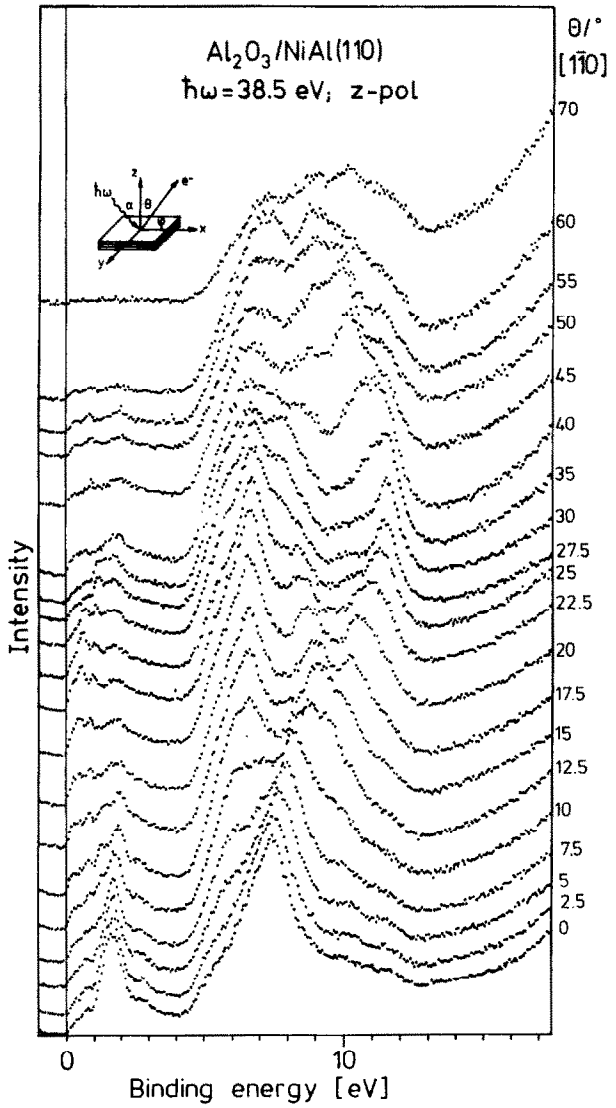

Fig. 10. Series of UP spectra of Al_2O_3/NiAl(110) (LEED pattern shown in fig. 2a) obtained at a fixed photon energy of 38.5 eV for different exit angles of the photoelectrons. The analyser was moved along the [1$\bar{1}$0] azimuth of the substrate.

levels dominate for the whole series, and that the substrate intensity is even further attenuated for increasing exit angles of the electrons. For an electron emission angle of 70° the substrate signal cannot be distinguished from noise. This is a rather qualitative indication that the adsorbate layer is smooth and covers up the whole substrate surface.

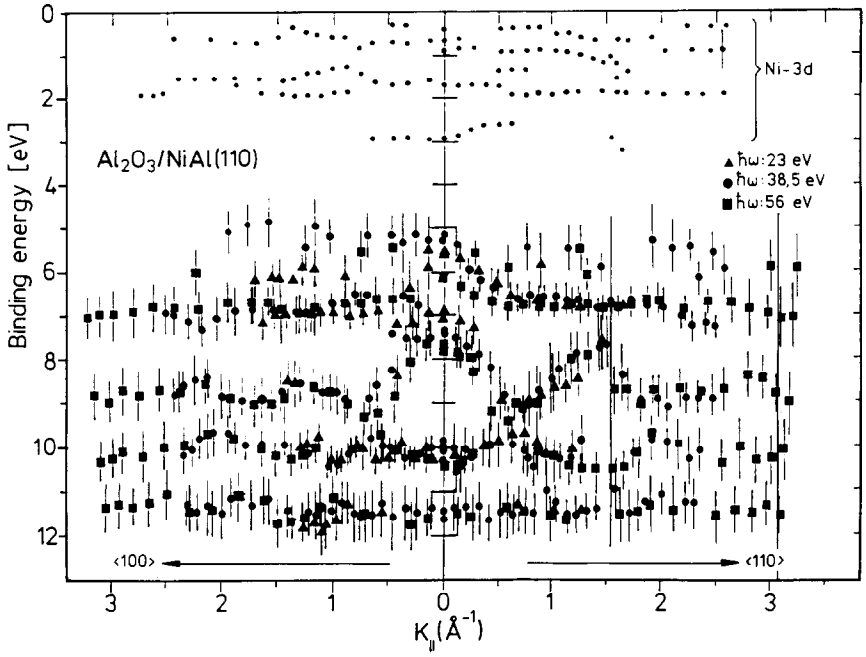

Fig. 11. Band structure of Al_2O_3/NiAl(110) determined along the [1$\bar{1}$0] and the [100] directions of the substrate. The LEED pattern of the oxide was that shown in fig. 2a.

There are further indications, however, that are strongly in favour of a closed adsorbate layer. One is the chemical inertness of the formed layer: NiAl(110) itself is an extremely reactive surface in that it is easy to contaminate and adsorbate induced features are readily seen in the photelectron spectra. After oxygen treatment, however, the surface appears to be inert even up to 800 K. If parts of the NiAl-surface were uncovered, we should be able to detect this.

Further experimental evidence is gained from the analysis of the angle-resolved photoemission data of fig. 10. From these data and other data taken at photon energies of 23, 38.5 and 56 eV the band dispersions shown in fig. 11 have been extracted. The k-vector was varied along the two high symmetry directions of the NiAl substrate, i.e., along [1$\bar{1}$0] and [001]. Different symbols for the data points are used for different photon energies. The small circles plotted close to the Fermi energy ($E_F \leq E_B \leq 3$ eV) are features due to the NiAl substrate. The electronic levels of the oxide between 5 and 12 eV binding energy exhibit rather pronounced dispersions of up to 2–3 eV for some of the bands along both, the [1$\bar{1}$0] and the [001] azimuth. The correspondence of the reciprocal space of the adlayer to that of the substrate is shown in fig. 12: The corners of the first Brillouin zone of the NiAl(110) substrate are

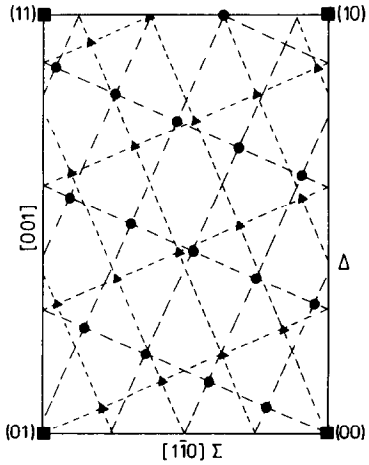

Fig. 12. Schematic showing the correspondence of the NiAl(110) substrate reciprocal space to that of aluminium oxide film for the two different domains of the oxide.

indicated by large squares, and the unit meshes of the two overlayer domains are marked by circles and triangles, respectively. The two high-symmetry directions of the substrate, i.e., [1$\bar{1}$0] and [001], are mirror lines for the oxide film in that sense that the mirror operations project one domain of the oxide film onto the other. Thus the substrate high-symmetry directions are equivalent directions for both oxide domains and the dispersions of the electronic states of the oxide along these directions in k-space should be the same for both domains. As can be seen from fig. 12 the dispersion periodicity observed for the oxide film along [1$\bar{1}$0] should be the same than the dispersion periodicity of the substrate whereas along [001] this should be not the case. Along [1$\bar{1}$0] the dispersion should be rather well defined. Starting from the center of the substrate Brillouin zone and varying the k-vector along [1$\bar{1}$0] (Σ) it can be seen from fig. 12 that the Γ points of the overlayer move away from the Σ line until the center of this line is reached and then move nearer again in a symmetric manner. Thus a dispersion with an energetic maximum, respectively minimum at the center of the substrate Brillouin zone along [1$\bar{1}$0] can be expected. Along [001] the dispersion behaviour should be somewhat more complicated because there are several Γ points of the oxide film near to the Δ line of the substrate.

Along the [1$\bar{1}$0] azimuth we determined the dispersions with respective maxima and minima up to a k-vector of about 3 Å^{-1} which is close to the boundary between the second and the third Brillouin zone of the NiAl(110) substrate unit cell. This is an unusually large range for an overlayer band structure and is indicative of the long-range order within the aluminium oxide overlayer. Vertical lines in fig. 11 mark the symmetry points for the overlayer as discussed above and it is quite obvious, that at least within the first substrate Brillouin zone the positions match more or less perfectly with the extrema of the dispersion curves. In the second substrate Brillouin zone the match is inferior, but this is most likely due to experimental uncertainties, i.e., energy and angular resolution connected with data taken at high photon energies and large off-normal exit angles. Along the [001] azimuth the dispersion is

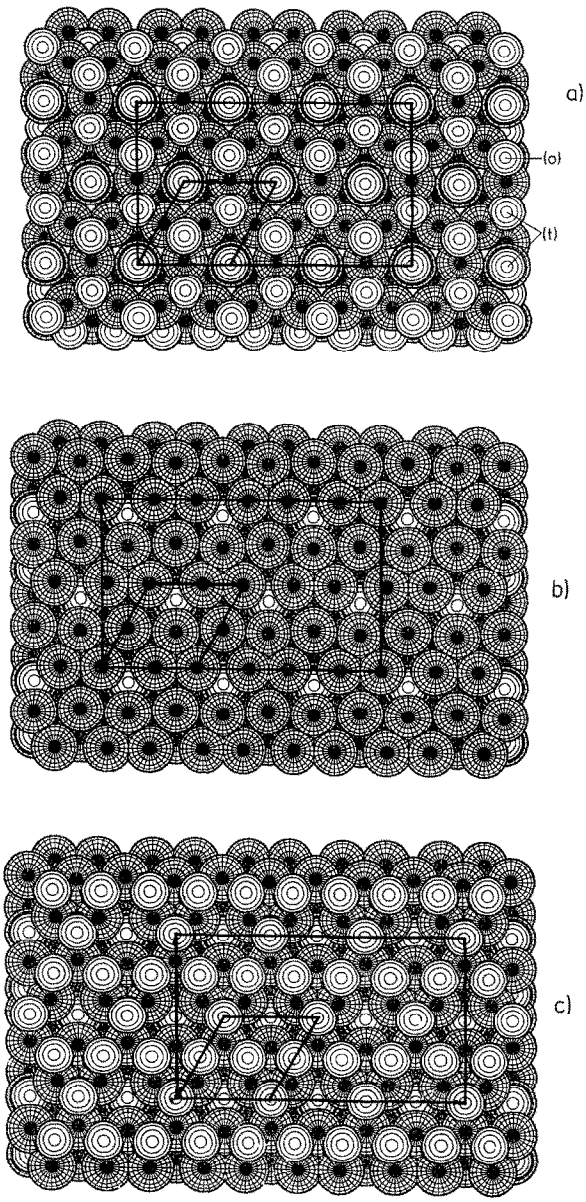

Fig. 13. Top views of the three different surface terminations of γ-Al_2O_3(111). For this plot the arrangement of atoms at the surfaces has been chosen to be the same as in the bulk. The lattice constants of the oxide have been modified such that the oxide film fits into the unit cell of Al_2O_3/NiAl(110) as determined by LEED (fig. 2a). For clarity all Al sites are occupied. (a) Al surface termination with mixed octahedral (o) and tetrahedral (t) Al sites. (b) Oxygen surface termination. (c) Al surface termination with exclusively octahedral Al sites. The notation octahedral and tetrahedral corresponds to bulk γ-Al_2O_3.

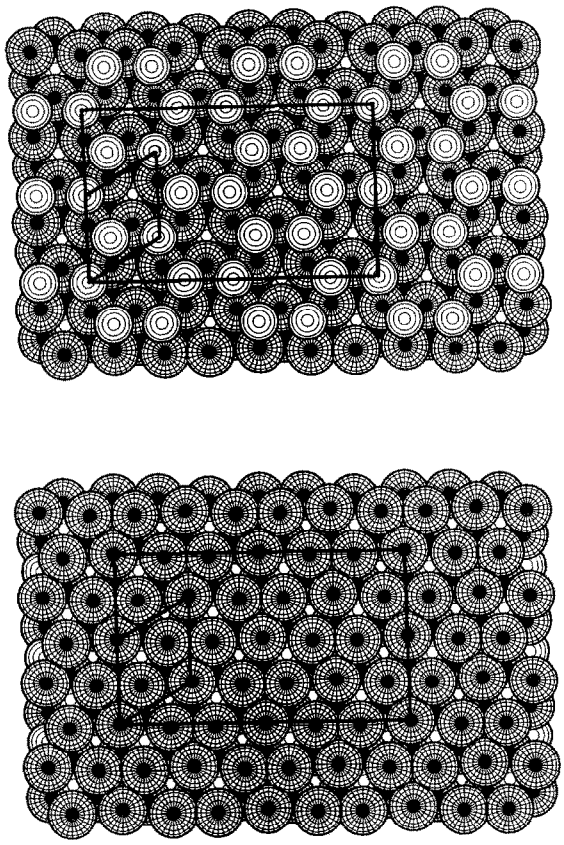

Fig. 14. Top views of the two different surface terminations of α-Al_2O_3(0001). For this plot the arrangement of atoms at the surfaces has been chosen to be the same as in the bulk. The lattice constants of the oxide have been modified such that the oxide film fits into the unit cell of Al_2O_3/NiAl(110) as determined by LEED (fig. 2a). (a) Al surface termination. (b) oxygen surface termination.

not so well defined as has to be expected from the above remarks. An alternative explanation for the observed dispersions is that they reflect the local arrangement of the oxygen atoms on the surface. As will be discussed in more detail in the following section we have fitted the quasi-hexagonal α-Al_2O_3(0001) and γ-Al_2O_3(111) surfaces into the oxide unit cell by enlarging the oxide lattice constants (figs. 13 and 14). For the distorted α-Al_2O_3(0001) surface the lengths of the resulting primitive reciprocal lattice vectors are about 1.37 $Å^{-1}$ which fits well to the observed dispersion periodicity. For γ-Al_2O_3(111) the surface structure is different and the reciprocal lattice vectors are shorter (about 1.2 $Å^{-1}$). In this case the match is inferior.

The next step is to try to interpret the observed band structure. Clearly, a detailed interpretation may only be carried out on the basis of quantitative band structure calculations. In the absence of this information we may still, however, try to deduce a qualitative picture from the experimental work:

We had already noted above that the photoemission data are not compatible with the formation of NiO on the surface. However, they are compatible with the formation of aluminium oxide. First, the published XPS work on Al_2O_3 [32,44,45] shows features in the same region as found in the present study. Secondly, the published calculated band width of 6 eV for the electronic levels of α-Al_2O_3 [42] is in perfect agreement with our data.

The bandwidth is basically determined by the numbers and distances of nearest and next nearest neighbours a given atom has. Therefore the similarity between the calculated Al_2O_3 bandwidth and the bandwidth observed in the present system is very strong indication that the coordination and the arrangement of the oxygen atoms is similar in both systems. Unfortunately, it is not possible to compare in a straight forward fashion the measured dispersion curves with the calculated band structure for bulk α-Al_2O_3 because the oxide film is so thin that it does not show a three-dimensional bulk band structure.

Fig. 11 only shows dispersions for five bands. There are two weakly or non-dispersing bands between 5.5 and 7 eV binding energy, followed by one strongly dispersing band between 7 and 9.5 eV. Between 10 and 11.5 eV there are finally again two weakly dispersing bands.

The model for the structure of the oxide film as indicated by the experimental data is a structure similar to that of the hexagonal γ-Al_2O_3(111) or α-Al_2O_3(0001) surfaces. This model will be discussed in more detail at the end of this paper. In the following discussion only the structure of γ-Al_2O_3(111) will be considered since the arguments for α-Al_2O_3(0001) are similar. As dis-

cussed before the oxide film is approximately 5 Å thick which corresponds to two oxygen layers and two Al layers. As shown in fig. 13 the oxygen layers of γ-Al_2O_3 are slightly distorted. Due to this distortion the two-dimensional hexagonal unit cell (the small unit cell in fig. 13) of each of the oxygen layers contains not one but four oxygen atoms. Considering that the oxide film consists of two aluminium layers and two oxygen layers we find that for the whole oxide film this unit cell contains 8 oxygen atoms and $5\frac{1}{3}$ Al atoms. That the latter value is not integer is due to the fact that in γ-Al_2O_3 not all Al sites are occupied. Thus this number only denotes the average number of Al atoms per unit cell. Since the 3p levels of the Al ions are empty we have to expect 24 bands derived from the p_x, p_y and p_z orbitals of the completely filled 2p levels of the 8 oxygen ions. In this discussion the fact that the real unit cell of the oxide is the large cell shown in fig. 2b has been neglected, assuming that the additional distortions leading to this unit cell are small. Out of the 24 band expected on the basis of the above considerations we could follow the dispersions of five bands through k-space. The reason that we could resolve only five bands might be that the deviation from true hexagonality with only 2 oxygen atoms per unit cell is so small that we could not resolve the additional splittings of the bands. Depending on whether the bands are formed from p-orbitals oriented perpendicular to the surface or from p-orbitals oriented within the surface plane different dispersion behaviour can be expected. For example, bands formed from s, or p_z orbitals would start at higher binding energies at Γ and disperse towards lower binding energies, while $p_{x,y}$-orbitals should exhibit the opposite dispersion behaviour. This kind of reasoning may lead us to explain the observed dispersions but it is crucial to first establish a reasonable structure model of the whole system. Once this problem has been tackled one may try to carry out band structure calculations on this system and compare it with the measured dispersions.

We shall attempt in the next section to construct a crude structural model of the system on the basis of the accumulated experimental evidence presented in the last sections.

4. Conclusion: the structure model

In order to design a structural model of the system under consideration, we use the main conclusions of the accumulated experimental evidences which we have discussed in detail in the previous sections.

We propose that initially oxygen destroys the surface order at least within the first two atomic layers of NiAl, i.e., to a depth of about 4 Å. This is consistent with the complete disappearance of the substrate LEED pattern because of the diffuse scattering of the electron beam. For thermodynamic reasons outlined above aluminium oxide islands form, while the Ni remains in its reduced state. After annealing to 600 K a ring is observed in the LEED pattern. As discussed before this ring might correspond to a rotationally disordered hexagonal overlayer with a lattice constant of 3.07 Å. Trying to find out what structure on the surface could be responsible for this LEED pattern we calculated the number of oxygen atoms needed to form stoichiometric Al_2O_3 from the aluminium atoms in the first two NiAl layers. If these oxygen atoms are arranged to form two hexagonal layers the lattice constant of these layers would be 3.01 Å. This is rather close to the 3.07 Å calculated from the diameter of the ring observed in LEED and not far away from typical oxygen–oxygen spacings observed for the different modifications of Al_2O_3, which are about 2.8 Å [33,46–50]. Following this we interpret the ring observed in the LEED pattern as an indication of the existence of such hexagonal oxygen layers on the surface. The existence of more or less distorted hexagonal oxygen layers is a common feature of nearly all of the many modifications of Al_2O_3 [33,46–50]. For γ-Al_2O_3 for instance such a layer corresponds to the oxygen terminated (111) surface (fig. 13) whereas for α-Al_2O_3 it is the (0001) surface which is quasi-hexagonal (fig. 14). We know from EELS and from LEED that after annealing a well ordered overlayer with a large unit cell which is rotated by 24° with respect to the substrate unit cell is formed. This layer has a thickness of approximately 5 Å as revealed by AES [11], XPS and ARUPS. This thickness nicely corresponds to two aluminium/

oxygen bilayers of γ-Al_2O_3(111), respectively α-Al_2O_3(0001) [33]. Although the LEED pattern of the thin film oxide is rather complex and at first sight does not seem to be due to a quasi-hexagonal oxide overlayer the distribution of intensities in the LEED pattern (see fig. 2a) clearly shows maxima which are arranged to form a hexagon. This is what has to be expected for a distorted hexagonal overlayer since the largest Fourier coefficients of the overlayer structure should correspond to the hexagonal base structure. But there is one open question, i.e., what happened to the Ni atoms of the first two NiAl layers? The ARUP spectra of the oxide film do not show any evidence for the formation of Ni–O interactions, i.e., NiO or $NiAl_2O_4$, nor any features which could be attributed to elemental Ni existing somewhere in the region of the Al_2O_3-NiAl interface. Our interpretation is that the Ni atoms are dissolved into the NiAl bulk during the annealing process which ordered the overlayer. This is rather probable since it is known that Ni is easily dissolved into NiAl at elevated temperatures. At 1250 K for instance the diffusion coefficient is 5×10^{-11} cm^2/s [51] which is sufficient for an appreciable extent of nickel diffusion into the NiAl bulk. This dissolution probably is one of the reasons for the ordering of the Al_2O_3 overlayer at high temperatures.

The overlayer is chemically inert as tested with a variety of molecules up to 800 K. This is a very strong indication that the film is compact and covers the substrate completely. The presumption that the oxide film is oxygen terminated is supported by the chemical inertness of the film because the electronic structure of O^{2-} is near to that of a rare gas and so the oxygen layer should be rather inert with respect to reaction with closed shell molecules or electropositive reactants, so that the sequence of layers is most likely NiAl–Al–O–Al–O. This conclusion is compatible with the ARUPS and XPS data. The experimentally determined bandwidths of the electronic levels of the aluminium oxide overlayer are in good agreement with theoretical estimates carried out on α-Al_2O_3 [42], which is not too different in structure from γ-Al_2O_3 concerning the lateral arrangement of the oxygen atoms. γ-Al_2O_3 contains tetrahedrally and octahedrally coordinated Al atoms [33], where the octahedral sites are not all occupied. If we assume that the arrangement of atoms at the surface does not differ from the arrangement in the bulk then for the (111) surface of γ-Al_2O_3 three different possible terminations exist, two terminations with only Al atoms in the top layer and one oxygen-terminated surface. These surfaces are shown in fig. 13. α-Al_2O_3 contains only octahedrally coordinated aluminium atoms. The two different (0001) surfaces of this oxide structure are shown in fig. 14. The unit cell of the oxide overlayer as determined by LEED and the primitive unit cells of the respective oxide structures are introduced into the figures. The dimensions of the unit cell of the oxide film correlate with the dimensions of the Al_2O_3 structures if the lattice constants are enlarged by 9.5% in one direction and by 6.7% in the other hexagonal direction for γ-Al_2O_3 and by 10.7%, respectively 7.9% for α-Al_2O_3. It turns out that within the area of the adlayer unit cell the oxide film contains 32 aluminium atoms and 48 oxygen atoms. The first number agrees well with the number of Al atoms in the first two NiAl(110) layers which have been oxidized to form Al_2O_3 according to the model developed above and in accordance with this model and the LEED observations the average lateral oxygen–oxygen spacings for these structures are 3.01 Å. The enlargement of the lattice constants of the film as compared to bulk Al_2O_3 might be driven by forces within the film. Rough estimates show that the average Madelung potential energy in the thin film is reduced as compared to the bulk. This would lead to enlarged lattice constants since the lattice constants of ionic compounds are determined by the balance of the attractive Madelung potential energy versus the repulsive potential of the ions.

One might ask how the enlargement of the lattice constants is reflected in the spectra of the oxide film. This question is not easily to be answered since the oxide film is so thin that it can not simply be considered as a bulk oxide with enlarged lattice constants. Concerning UPS it has already been shown that the band structure of the oxide film is only two-dimensional whereas

the band structure of bulk Al_2O_3 is of course three-dimensional. There are similar problems for EELS. Thus only high qualitative calculations for this thin oxide film might allow to tackle this problem by comparison with the experimental data.

The remaining problem is: Is it possible to rationalize the observed orientation, i.e., the rotation of the unit cell by 24° with respect to the NiAl substrate? The fact that the adlayer is incommensurate with the substrate in one direction indicates that the oxide–substrate interaction is weaker than the lateral interactions within the oxide, which is an additional indication that the enlargement of the lattice vectors of the thin oxide film as compared to the lattice vectors of bulk Al_2O_3 is mainly not due to interaction with the substrate but an intrinsic property of this thin film. Although the oxide–substrate interaction is weaker than the lateral interaction within the oxide the oxide film will try to establish some sort of commensurability if this is possible. This presumably leads to the observed commensurability with the substrate along the [1$\bar{1}$0] direction. Without distorting the oxide film too much this can be achieved by arranging the oxide unit cell as shown in fig. 2b. In this case the lengths of the two lattice vectors of the quasi-hexagonal base structure of the oxide film parallel to the surface differ only by 2.6%, which means that the distortion of the base structure is rather weak.

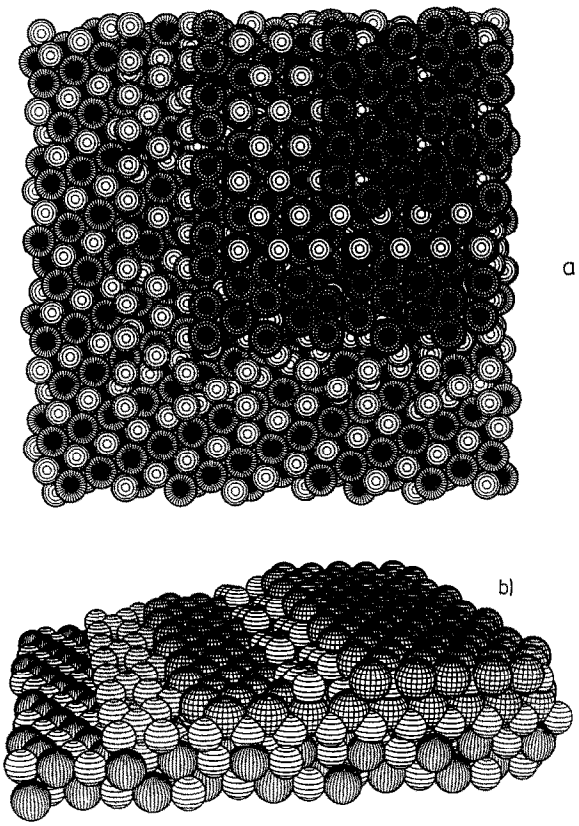

Fig. 15. Structure model for γ-Al_2O_3(111)/NiAl(110). (a) Top view. (b) Perspective side view.

At this point we would like to discuss the significance of the structure model developed above. The main evidences for this model have been derived from LEED and EELS. LEED shows that the topmost layer of the oxide film must consist of oxygen atoms arranged in a quasi-hexagonal manner. We feel that this evidence is rather conclusive but it is not sufficient to assign the structure of the layer definitely since nearly all of the many modifications of Al_2O_3 contain quasi-hexagonal oxygen layers with similar lattice constants [33,46–50]. We have tried to fit the structures of α-Al_2O_3(0001) and γ-Al_2O_3(111) into the oxide unit cell of Al_2O_3/NiAl(110). The results are shown in the figs. 15 and 16, respectively. The EELS spectra fit better to γ-Al_2O_3 since the calculated loss function (fig. 6) of this aluminium oxide modification agrees well with the EEL spectra of the oxide film (fig. 4) as evident by the existence of the loss at 400 cm^{-1}. However, it should be noted that calculations of Rhodin and coworkers [26] for a thin film of α-Al_2O_3, terminated by vacuum on one side and by metal on the other side also show the mode at 400 cm^{-1} so that the EELS data might also be consistent with α-Al_2O_3. Thus we conclude that the arrrangement of the oxygen atoms in the thin film is rather clear whereas the arrangement of the aluminium atoms is not. One interesting point to mention is that the orientation of the hexagonal ring fragments in the LEED patterns shown in figs. 1c and 1d differs from the orientation of the hexagonal intensity distribution in the final LEED pattern (fig. 2a) by 30°. This

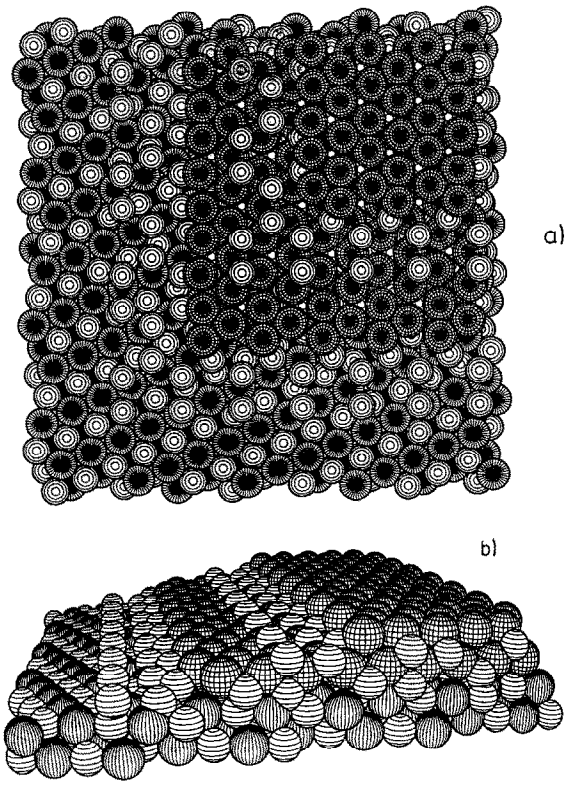

Fig. 16. Structure model for α-Al_2O_3(0001)/NiAl(110). (a) Top view. (b) Perspective side view.

indicates that there must be some sort of phase transition in the overlayer.

The two structure models considered so far, i.e., the structures of α-Al_2O_3(0001) and γ-Al_2O_3(111) on NiAl(110), are shown in figs. 15 and 16 in a quasi three-dimensional representation. For the individual interlayer distances of γ-Al_2O_3 we have choosen 1 Å between the oxygen layers and that Al layer which only contains octahedrally coordinated Al atoms and 1.28 Å between the other type of Al layer and the oygen layers as known from literature [33]. For α-Al_2O_3 the characteristic distance is 1.08 Å which is the distance between the oxygen and the aluminium layers. The distance between the lowest Al layer and the topmost NiAl layer should be considerably smaller than the Ni–NiAl separation. In fact it should be rather similar to the oxygen–Al separation considering covalent radii. We assume a value of 1.2 Å for this distance. Adding the various interlayer distances we get 4.5 Å for the separation between the topmost oxygen layer and the topmost NiAl layer. Such a layer thickness is compatible with the experimental findings.

5. Summary

We have employed different electron spectroscopic techniques to investigate the structure of a thin film of Al_2O_3 epitaxially grown on NiAl(110). The main structural informations are derived from our LEED data which show that the Al_2O_3 film most likely contains distorted hexagonal oxygen layers. The oxygen–oxygen spacings are slightly enlarged as compared with typical oxygen–oxygen spacings of bulk Al_2O_3. From our XPS data and AES data reported in literature [11] we know that the thickness of the film is about 5 Å, in agreement with the ARUPS data which revealed that the electronic band structure of the adlayer is only two dimensional, and the EELS data suggest that the structure of the oxide film is most likely similar to that of γ-Al_2O_3 or α-Al_2O_3. Putting together these results we were able to build up a structural model for the oxide film. According to this model the structure of the oxide film is similar to that of the α-Al_2O_3(0001) or γ-Al_2O_3(111) surfaces, respectively. The thickness of the film is compatible with two bilayers consisting of an aluminium layer and a quasi-hexagonal oxygen layer, most likely with oxygen surface termination as deduced from the chemical inertness of the film.

Acknowledgements

This work has been funded by the Deutsche Forschungsgemeinschaft (DFG) and the Bundesministerium für Forschung und Technologie (BMFT). HJF gratefully acknowledges financial support by the Fonds der Chemischen Industrie. We thank the Max-Planck-Institut für Eisenforschung for providing us with an excellent NiAl single-crystal rod. This publication has been initiated by H.J.F. and M.W. during a stay in Prof. G. Somorjai's group in Berkeley, California. We thank Prof. G. Somorjai for his kind hospitality.

Prof. K. Müller is gratefully acknowledged for helpful discussions and we thank A. Rizzi and A. Förster for providing us with calculations for the oxide energy loss function.

References

[1] M. Liehr and P.A. Thiry, J. Electron Spectrosc. Relat. Phenom. 54/55 (1990) 1013.
[2] J.L. Erskine and R.L. Strong, Phys. Rev. B 25 (1982) 5547.
[3] R.L. Strong, B. Firey, F.W. de Wette and J.L. Erskine, Phys. Rev. B 26 (1982) 3483; J. Electron Spectrosc. Relat. Phenom. 29 (1983) 187.
[4] J.E. Crowell, J.G. Chen and J.T. Yates, Jr., Surf. Sci. 165 (1986) 37.
[5] J.G. Chen, J.E. Crowell and J.T. Yates, Jr., Surf. Sci. 187 (1987) 243.
[6] R.L. Strong and J.L. Erskine, J. Vac. Sci. Technol. A 3 (1985) 1428.
[7] R. Michel, J. Gastaldi, C. Allasia, C. Jourdan and J. Derrien, Surf. Sci. 95 (1980) 309.
[8] J.G. Chen, J.E. Crowell and J.T. Yates, Jr., Phys. Rev. B 35 (1987) 5299; Phys.Rev. B 33 (1986) 1436.
[9] J. Doychak, J.L. Smialek and T.E. Mitchell, Metall. Trans. A 20 (1989) 499.
[10] K. Müller, H. Lindner, D.M. Zehner and G. Ownby, Verh. Dtsch. Phys. Ges. 25 (1990) 1130;
K. Müller, H. Lindner, D.M. Zehner and G. Ownby, private communication.
[11] H. Isern and G.R. Castro, Surf. Sci. 211/212 (1989) 865.
[12] H. Ibach, Electron Energy Loss Spectrometers, Springer Series in Optical Sciences (Springer, Berlin, 1990).
[13] M. Hansen, Constitution of Binary Alloys (McGraw-Hill, New York, 1958) pp. 118–121.
[14] M.H. Kang and E.J. Mele, Phys. Rev. B 36 (1987) 7371.
[15] H.L. Davis and J.R. Noonan, Phys. Rev. Lett. 54 (1985) 566;
H.L. Davis and J.R. Noonan, J. Vac. Sci. Technol. A 3 (1985) 1507.
[16] S.M. Yallisove and W.R. Graham, Surf. Sci. 183 (1987) 556.
[17] M. Wuttig, W. Hoffmann, E. Preuss, R. Franchy, H. Ibach, Y. Chen, M.L. Xu and S.Y. Tong, Phys. Rev. B 42 (1990) 5443.
[18] M. Wuttig, W. Hoffmann, E. Preuss, R. Franchy and H. Ibach, Vacuum 41 (1990) 433.
[19] Small peak shifts are due to an isotope effect, i.e., the spectrum in fig. 4 has been produced by adsorption of O^{18} instead of O^{16}. This leads to a frequency decrease of 5.7% assuming no anharmonic contributions.
[20] R. Franchy, M. Wuttig and H. Ibach, Surf. Sci. 189/190 (1987) 438.
[21] A.M. Venezia and C.M. Loxton, Surf. Sci. 194 (1988) 136.
[22] G. Dalmai-Imelik, J.C. Bertolini and J. Rousseau, Surf. Sci. 63 (1977) 67.
[23] H. Kuhlenbeck, G. Odörfer, R. Jaeger, G. Illing, M. Menges, Th. Mull, H.-J. Freund, M. Pöhlchen, V. Staemmler, S. Witzel, C. Scharfschwerdt, K. Wennemann, T. Liedtke and M. Neumann, Phys. Rev. B 43 (1991) 1969.
[24] M. Liehr, P.A. Thiry, J.J. Pireaux and R. Caudano, J. Vac. Sci. Technol. A 2 (1984) 1079.
[25] A. Rizzi and A. Förster, private communication.
[26] B.G. Frederick, G. Apai and T.H. Rhodin, Surf. Sci. 244 (1991) 67.
[27] D.Y. Smith, E. Shiles and M. Inokuti, Handbook of Optical Constants of Solids (Academic Press, New York, 1985) p. 395.
[28] P.J. Chen, M.L. Colaianni and J.T. Yates, Jr., Phys. Rev. B 41 (1990) 8025.
[29] P. Steiner, H. Höchst and S. Hüfner, Z. Phys. B 30 (1978) 129.
[30] P.H. Citrin, G.K. Wertheim and Y. Baer, Phys. Rev. B 16 (1977) 4256.
[31] R. Kammerer, J. Barth, F. Gerken, C. Kunz, S.A. Flodström and J.I. Johansson, Phys. Rev. B 26 (1982) 3491.
[32] D. Nicolas-Chaubet, C. Haut, C. Picard, F. Millot and A.M. Huntz, Mater. Sci. Eng. A 120 (1989) 83.
[33] K.P. Sinha and A.P.B. Sinha, J. Phys. Chem. 61 (1957) 758.
[34] CRC Handbook of Chemistry and Physics, 52th ed., (CRC Press, Boca Raton, FL, 1971/1972).
[35] Metals Handbook, 8th ed., Vol. 8, Ed. Taylor Lyman (American Society of Metals, Metals Park, OH, 1973).
[36] J.H. Sinfelt, Sci. Am. 253 (1985) 96.
[37] M.H. Kang, S.-C. Lui, E.J. Mele, E.W. Plummer and D.M. Zehner, Phys. Rev. B 41 (1990) 4920.
[38] S.-C. Lui, PhD Thesis, University of Pennsylvania, USA, 1988.
[39] S.-C. Lui, J.W. Davenport, E.W. Plummer, D.M. Zehner and G.W. Fernando, Phys. Rev. B 42 (1990) 1582.
[40] S.-C. Lui, M.H. Kang, E.J. Mele, E.W. Plummer and D.M. Zehner, Phys. Rev. B 39 (1989) 13149.
[41] Z.-X. Shen, C.K. Shih, O. Jepsen, W.E. Spicer, I. Lindau and J.W. Allen, Phys. Rev. Lett. 64 (1990) 2442.
[42] I.P. Batra, J. Phys. C15 (1982) 5399.
[43] K.-P. Kämper, W. Schmitt, G. Güntherodt and H. Kuhlenbeck, Phys. Rev. B 38 (1988) 9451.
[44] J.A. Ramsey, Appl. Surf. Sci. 13 (1982) 159.
[45] J. Stöhr, L.I. Johansson, S. Brennan, M. Hecht and J.N. Miller, Phys. Rev. B 22 (1980) 4052.
[46] H.D. Megaw, Crystal Structures: A Working Approach (Saunders, Philadelphia, 1973) pp. 226f.
[47] G. Yamaguchi, I. Yasui and Wen-Chau Chiu, Bull. Chem. Soc. Jpn. 43 (1970) 2487.
[48] Structure Reports 13 (1950) 223.
[49] Structure Reports 43 A (1977) 348.
[50] Gmelins Handbuch der anorganischen Chemie, 8th ed. (Verlag Chemie, Weinheim, 1953) p. 78.
[51] G.F. Hancock and B.R. McDonnell, Phys. Status Solidi (a) 4 (1971) 143.